THE ASTRONOMICAL JOURNAL, 125:3366–3377, 2003 June

143P/KOWAL-MRKOS AND THE SHAPES OF COMETARY NUCLEI

DAVID JEWITT, SCOTT SHEPPARD, AND YANGA FERNÁNDEZ
Institute for Astronomy, 2680 Woodlawn Drive, Honolulu, HI 96822-1897;
jewitt@ifa.hawaii.edu, sheppard@ifa.hawaii.edu, yan@ifa.hawaii.edu
Received 2003 January 13; accepted 2003 February 19

ABSTRACT

We add 143P/Kowal-Mrkos to the small but growing sample of well-observed cometary nuclei. Photometric observations from 3.4 to 4.0 AU heliocentric distance reveal a pointlike object with no detectable outgassing. Periodic modulation of the scattered light ($\Delta m_R = 0.45 \pm 0.05$) is attributed to rotation of the bare nucleus with a double-peaked period 17.21 ± 0.10 hr and a projected ratio of the shortest to longest axis of about 0.67/1. We also measured the phase coefficient (0.043 ± 0.014 mag deg^{-1}), the *BVRI* colors ($V-R = 0.58 \pm 0.02$), and the absolute red magnitude [$m_R(1, 1, 0) = 13.49 \pm 0.20$]. The effective circular radius is 5.7 ± 0.6 km (geometric albedo 0.04 assumed). We study the properties of 11 well-observed Jupiter-family comet (JFC) nuclei. On average, the nuclei are systematically more elongated (average photometric range $\Delta m_R = 0.54 \pm 0.07$) than main-belt asteroids of comparable size ($\Delta m_R = 0.32 \pm 0.05$) and more elongated than fragments produced in laboratory impact experiments. We attribute the elongation of the nuclei to an evolutionary effect, most likely driven by sublimation-induced mass loss. However, we find no evidence for any relation between the nucleus shape and the sublimation timescale. This may be because the timescale for evolution of the nucleus shape is very short compared with the dynamical timescale for the JFCs, meaning that most nuclei in our sample are already highly physically evolved.

Key words: comets: general — comets: individual (143P/Kowal-Mrkos) — Kuiper belt

1. INTRODUCTION

Jupiter-family comets (JFCs) are low-inclination comets that are dominated by gravitational interactions with Jupiter (Tisserand parameters $2 < T_J < 3$). The nuclei of the JFCs are now thought to be fragments of larger, parent objects produced by collisions in the Kuiper belt (Farinella & Davis 1996). Ejection of solid matter from the nuclei occurs in response to sublimation-driven outgassing of trapped volatiles, predominantly water ice. Large solid particles cannot be ejected against the nucleus gravity and may remain behind to form a "rubble mantle" that progressively restricts the gas flow from the nucleus. The few well-observed JFC nuclei sublimate from only a tiny fraction of the geometric surface, typically 0.1%–10%, with refractory matter mantling the remainder (A'Hearn et al. 1995). The sublimation lifetime of a comet is typically less than its dynamical ejection time. This means many dead or nearly dead comets should exist that are not easily distinguished from near-Earth asteroids by current observational methods (Luu & Jewitt 1990). Recent albedo measurements show that the dead comets make up ~10% of the near-Earth object population, but this fraction is very uncertain (Fernández, Jewitt, & Sheppard 2001).

Scientific interest in the JFCs focuses on their assumed role as samples of primitive matter from the outer reaches of the solar accretion disk, as projectiles responsible for cratering the exposed surfaces of planets and satellites throughout the solar system, as the deliverers of volatiles to the terrestrial planets (Laufer et al. 1999), and as sources of interplanetary dust. We also wish to know the distribution of the physical properties of the JFCs (especially size, albedo, shape, rotation, and spectral nature) in order to understand their relation to the precursor Centaur and Kuiper belt populations. Unfortunately, cometary nuclei are small, dark, and (usually) enveloped in a gas and dust coma whose scattering cross section exceeds that of the solid nucleus. Reliable physical observations of nuclei are difficult to obtain, and few examples exist in the published literature. Therefore, 50 years after the basic physics of these objects was first described (Whipple 1950), it remains useful to document observations of even a single bare cometary nucleus, as is our objective in the present paper.

Comet 143P/Kowal-Mrkos was discovered in 1984 (Kowal & Mrkos 1984). It is a JFC, with semimajor axis $a = 4.309$ AU, eccentricity $e = 0.409$, and inclination $i = 4.^\circ7$ (the Tisserand parameter is $T_J = 2.87$). The orbit is Jupiter-crossing, and the long-term dynamics are controlled by strong perturbations from this planet. In ~1630, a Jupiter encounter raised the perihelion from about 1 to 1.9 AU (Carusi et al. 1985). It passed 0.16 AU from Jupiter in 1989, which further raised the perihelion from 1.9 AU to the present 2.5 AU (Marsden 2000). No quantitative physical observations of this object have been published.

In the following sections we first present and discuss the new observational results pertaining to 143P/Kowal-Mrkos. Then we more generally discuss what is known about the shapes of cometary nuclei, drawing on the best results from the literature as our database.

2. OBSERVATIONS

Observations were taken in 2001 June and November at the f/10 Cassegrain focus of the University of Hawaii 2.2 m telescope atop Mauna Kea. A Tektronix 2048 × 2048 pixel CCD camera was used, giving an image scale of $0.''219$ pixel^{-1}. Broadband *BVRI* filters approximating the Johnson-Kron-Cousins photometric system were employed, with the bulk of the data taken in the *R* filter, corresponding to the peak quantum efficiency (~0.9) of the CCD. The telescope was tracked at nonsidereal rates to

TABLE 1
GEOMETRIC CIRCUMSTANCES OF THE OBSERVATIONS

UT Date (2001)	R (AU)	Δ (AU)	α (deg)	Δ/c[a] (minutes)
Jun 18	3.396	2.475	8.5	20.58
Jun 19	3.400	2.472	8.2	20.55
Jun 20	3.404	2.469	7.9	20.53
Jun 28	3.433	2.455	5.5	20.41
Jun 29	3.437	2.454	5.1	20.41
Jun 30	3.440	2.454	4.8	20.41
Nov 17	3.957	4.332	12.7	36.03
Nov 18	3.960	4.349	12.6	36.17
Nov 19	3.964	4.365	12.5	36.30

[a] Light-travel time.

follow the motion of the comet (at $\sim 21'' \text{ hr}^{-1}$ in 2001 June). The images had a point-spread function of 0.″7–0.″9 full width at half-maximum, with contributions from the atmosphere, the telescope optics, and a small periodic error in the telescope tracking drive. Most observations were taken in photometric conditions and were directly calibrated with reference standard stars of Sun-like color (Landolt 1992). Other observations taken through cirrus were calibrated retroactively, using background stars as a reference. The CCD systematics were removed using a bias measured by overclocking and a flat field constructed from the median of the night-sky images. Table 1 presents the geometric circumstances of the observations, while the photometry is presented in Table 2.

3. OBSERVATIONAL RESULTS

We compiled a stacked image from the shifted median of nine individual R-band images (total integration 2700 s) taken on 2001 June 19 in the interval UT 1109–1328. The seeing was about 0.″8 FWHM, and the background to the comet was relatively free of contaminating field stars. The radial profile is plotted in Figure 1, along with the corresponding profile of an unresolved field star. Since the comet images were tracked at nonsidereal rates, it was necessary to extract the field star profile from other, sidereally guided images of equal integration time. As a result, the field star reference profile does not sample exactly the same pattern of seeing or telescope shake as in the comet profile. Nevertheless, the profile shows no evidence of coma with a

TABLE 2
R-BAND PHOTOMETRY OF 143P/KOWAL-MRKOS

No.	UT Date (2001)	m_R[a]	No.	UT Date (2001)	m_R[a]	No.	UT Date (2001)	m_R[a]
1.....	Jun 18.4985	18.62	36.....	Jun 28.4506	18.42	71.....	Jun 30.3915	18.76
2.....	Jun 18.5107	18.63	37.....	Jun 28.4576	18.39	72.....	Jun 30.3969	18.78
3.....	Jun 19.3653	18.86	38.....	Jun 28.4604	18.42	73.....	Jun 30.4151	18.76
4.....	Jun 19.3699	18.81	39.....	Jun 28.4702	18.42	74.....	Jun 30.4198	18.75
5.....	Jun 19.3799	18.76	40.....	Jun 28.4760	18.44	75.....	Jun 30.4246	18.75
6.....	Jun 19.3846	18.73	41.....	Jun 28.4884	18.43	76.....	Jun 30.4294	18.71
7.....	Jun 19.3895	18.72	42.....	Jun 28.5303	18.51	77.....	Jun 30.4364	18.65
8.....	Jun 19.3946	18.67	43.....	Jun 28.5472	18.56	78.....	Jun 30.4459	18.67
9.....	Jun 19.3990	18.65	44.....	Jun 28.5520	18.58	79.....	Jun 30.4515	18.67
10.....	Jun 19.4038	18.66	45.....	Jun 28.5578	18.58	80.....	Jun 30.4998	18.55
11.....	Jun 19.4086	18.62	46.....	Jun 29.4094	18.61	81.....	Jun 30.5052	18.54
12.....	Jun 19.4133	18.63	47.....	Jun 29.4150	18.59	82.....	Jun 30.5099	18.50
13.....	Jun 19.4182	18.60	48.....	Jun 29.4198	18.56	83.....	Jun 30.5146	18.50
14.....	Jun 19.4231	18.62	49.....	Jun 29.4245	18.56	84.....	Jun 30.5193	18.53
15.....	Jun 19.4281	18.59	50.....	Jun 29.4300	18.55	85.....	Jun 30.5240	18.52
16.....	Jun 19.4425	18.53	51.....	Jun 29.4446	18.47	86.....	Jun 30.5744	18.45
17.....	Jun 19.4520	18.53	52.....	Jun 29.4514	18.48	87.....	Jun 30.5792	18.44
18.....	Jun 19.4569	18.53	53.....	Jun 29.4689	18.43	88.....	Jun 30.6027	18.44
19.....	Jun 19.4615	18.52	54.....	Jun 29.4795	18.41	89.....	Jun 30.6081	18.41
20.....	Jun 19.4666	18.52	55.....	Jun 29.4855	18.40	90.....	Nov 17.1942	20.51
21.....	Jun 19.4714	18.52	56.....	Jun 29.4977	18.39	91.....	Nov 17.1996	20.52
22.....	Jun 19.4762	18.52	57.....	Jun 29.5133	18.38	92.....	Nov 17.2048	20.53
23.....	Jun 19.4953	18.48	58.....	Jun 29.5388	18.37	93.....	Nov 17.2159	20.53
24.....	Jun 19.5002	18.47	59.....	Jun 29.5508	18.36	94.....	Nov 17.2272	20.38
25.....	Jun 19.5323	18.45	60.....	Jun 29.5585	18.36	95.....	Nov 17.2333	20.46
26.....	Jun 19.5392	18.48	61.....	Jun 29.5638	18.37	96.....	Nov 18.2037	20.54
27.....	Jun 19.5442	18.51	62.....	Jun 29.5903	18.37	97.....	Nov 18.2094	20.62
28.....	Jun 19.5488	18.49	63.....	Jun 29.5957	18.40	98.....	Nov 18.2154	20.57
29.....	Jun 19.5537	18.49	64.....	Jun 29.6005	18.39	99.....	Nov 18.2217	20.72
30.....	Jun 19.5585	18.52	65.....	Jun 30.3414	18.52	100.....	Nov 19.1959	20.22
31.....	Jun 19.5633	18.53	66.....	Jun 30.3461	18.54	101.....	Nov 19.2019	20.26
32.....	Jun 19.5682	18.54	67.....	Jun 30.3698	18.67	102.....	Nov 19.2078	20.24
33.....	Jun 20.3836	18.83	68.....	Jun 30.3746	18.69	103.....	Nov 19.2197	20.34
34.....	Jun 20.4749	18.66	69.....	Jun 30.3800	18.72	104.....	Nov 19.2257	20.39
35.....	Jun 28.4401	18.42	70.....	Jun 30.3857	18.75			

[a] Accuracy of the magnitudes is estimated at $1\sigma = 0.02$–0.03 mag.

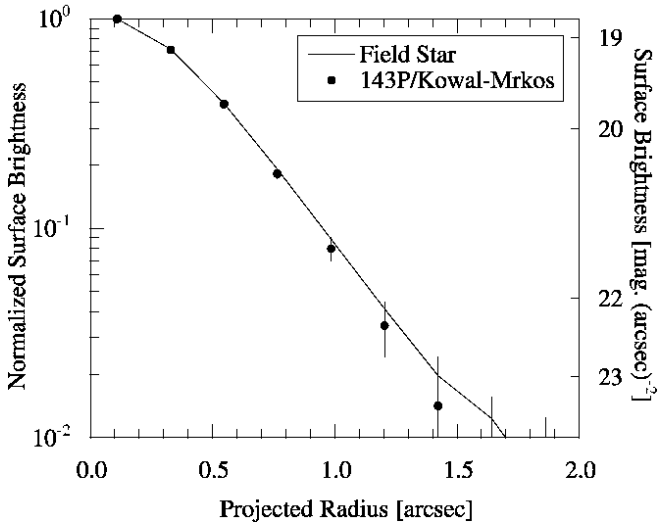

FIG. 1.—Normalized *R*-band surface brightness profile of P/Kowal-Mrkos on UT 2001 June 19 compared with that of an unresolved field star. The effective integration time is 2700 s. The peak of the comet profile has absolute surface brightness 18.8 mag arcsec^{-2} (*right axis*). Error bars show the result of uncertainty in the determination of the sky background adjacent to the comet.

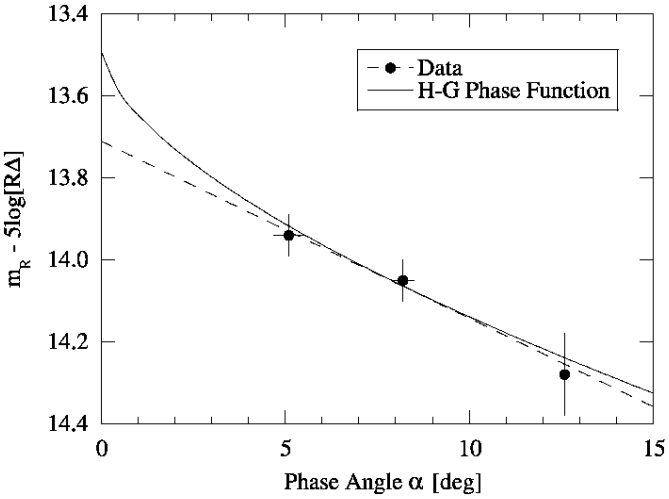

FIG. 2.—Mean apparent magnitude plotted against the phase angle of observation, for data taken in the mid June, late June, and November periods. The mean magnitudes have been corrected to unit heliocentric and geocentric distances using the inverse square law. The dashed line shows the least-squares fit phase coefficient $\beta = 0.043 \pm 0.014$ mag deg^{-1}, while the solid line shows a Bowell et al. (1989) type phase curve having $G = 0.15$, appropriate for a low-albedo solid body. We use the latter curve to extrapolate to zero phase angle.

surface brightness $\Sigma(\theta)$ greater than about 1% of the central surface brightness, corresponding to $\Sigma(1'') \geq 23.8$ mag arcsec^{-2} (Fig. 1), at $\theta = 1''$.

For a steady state coma in uniform outflow, the integrated magnitude $m_c(\theta)$ of the coma within radius θ is related to the surface brightness $\Sigma(\theta)$ at radius θ by

$$\Sigma(\theta) = m_c(\theta) + 2.5 \log 2\pi\theta^2 \quad (1)$$

(Jewitt & Danielson 1984). Substituting into equation (1) then gives $m_c(1'') \geq 21.8$. This is at least 3.3 mag (a factor of 20) fainter than the mean magnitude of the comet in the images used to measure the surface brightness profile, namely, $m_R = 18.5$. Therefore, we conclude that the surface brightness profile of Kowal-Mrkos provides no evidence for contamination by a steady state coma greater than about 5% of the measured signal. The radial profile places no useful constraints on possible near-nucleus coma ($\theta < 1''$, or about 1700 km) with a radial profile much steeper than in the steady state case.

The apparent magnitude of a body viewed in reflected sunlight is related to its observing geometry by

$$p_R \Phi(\alpha) r_n^2 = 2.24 \times 10^{22} R^2 \Delta^2 10^{0.4(m_\odot - m_R)} , \quad (2)$$

where p_R is the red (0.65 μm wavelength) geometric albedo, $\Phi(\alpha)$ is the phase function for phase angle α, r_n is the effective circular radius of the body, R (AU) and Δ (AU) are the heliocentric and geocentric distances, and $m_\odot$ and m_R are the apparent magnitudes of the Sun and the object. The phase function is conventionally expressed in several ways. Over limited ranges of phase angle, the function is well approximated by $\Phi(\alpha) = 10^{-0.4\beta\alpha}$, where the linear phase coefficient β (mag deg^{-1}) is estimated below. Near opposition, the scattering efficiency may display a surge that is better matched by more complicated functions, as described by Bowell et al. (1989). Our measurements of m_R at three epochs (i.e., three sets of R, Δ, and α) enable us to estimate both $\Phi(\alpha)$ and the product $p_R r_n^2$, but disentangling the albedo from the size requires additional information that we do not possess.

The mean magnitude of the comet, corrected for the varying heliocentric and geocentric distances, is plotted as a function of the phase angle in Figure 2. The uncertainties on the means reflect both the errors in the photometry and, particularly in the data from November, uncertainties resulting from incomplete coverage of the rotational light curve. A weighted least-squares fit to the data in Figure 2 (*dashed line*) shows that in the $5^\circ \leq \alpha \leq 12^\circ$ phase-angle range, the phase darkening is well represented by a linear coefficient $\beta = 0.043 \pm 0.014$ mag deg^{-1}. The magnitude of β is inversely related to the albedo (Belskaya & Shevchenko 2000): the large value found for 143P/Kowal-Mrkos suggests a low-albedo surface. The measured phase darkening falls within the range of other published values, namely, for P/Tempel 2 ($\beta = 0.04 \pm 0.01$ mag deg^{-1}; Jewitt & Luu 1989), P/Encke ($\beta = 0.05 \pm 0.02$ mag deg^{-1}; Fernández et al. 2000), and P/Neujmin 1 ($\beta = 0.025 \pm 0.006$ mag deg^{-1}; Delahodde et al. 2001).

The solid line in Figure 2 shows a Bowell et al. (1989) type phase curve having $G = 0.15$, as is appropriate for a low-albedo solid body. It fits the data within the uncertainties of measurement. We use equation (2) and the Bowell et al. phase function to estimate the absolute magnitude (the magnitude at $R = \Delta = 1$ AU and $\alpha = 0^\circ$) of Kowal-Mrkos as

$$m_R(1, 1, 0) = 13.49 \pm 0.20 . \quad (3)$$

The uncertainty on this number is introduced primarily by the extrapolation to $\alpha = 0$ (Fig. 2). Assuming $p_R = 0.04$, as found for other short-period comet nuclei (Jewitt 1991) and for objects believed (on dynamical grounds) to be dead comets (Fernández et al. 2001), equations (2) and (3) give the effective nucleus radius as

$$r_n = 5.7 \pm 0.6 \text{ km} , \quad (4)$$

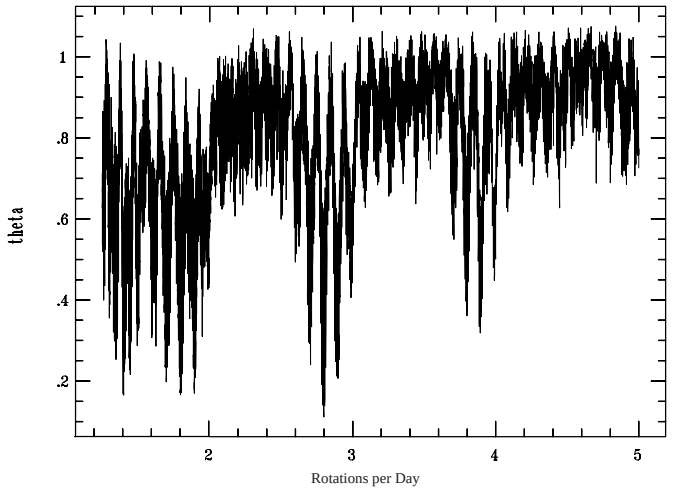

FIG. 3.—Phase dispersion minimization plot of the combined photometry. The minima spaced at about 0.1 day^{-1} result from aliasing between the mid-June and late-June photometry.

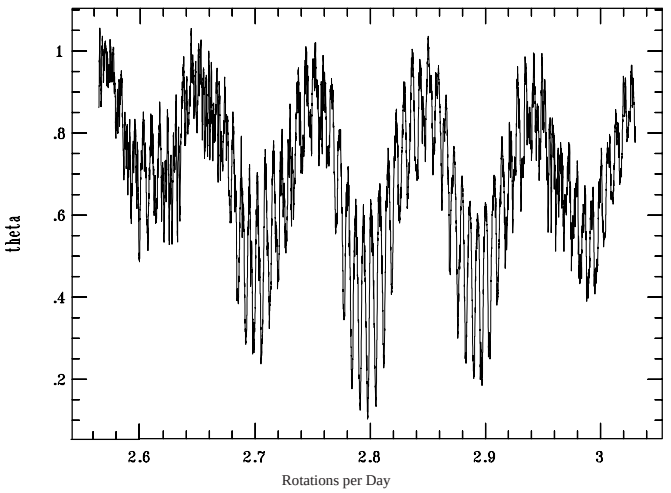

FIG. 4.—Same as Fig. 3, but at higher resolution to show substructure in the phase dispersion plot. The minima spaced at about 1/130 day^{-1} result from aliasing between the June and November photometry.

where the quoted error does not include uncertainty in the geometric albedo (a ±50% error in albedo corresponds to a ±25% error in the radius).

The nightly *R*-band photometry shows systematic variations that are larger than the photometric errors. We used phase dispersion minimization (PDM) to search for plausible periods in the photometry (Stellingwerf 1978). The data from UT 2001 June 18–20 and 28–30 provide the main constraint on the photometric period. Data from November incompletely sample the light curve and cannot be used by themselves to meaningfully isolate the period. Figure 3 shows the PDM plot computed from the combined data and including corrections for light-travel time and phase darkening.

The deepest minimum in Figure 3 occurs near rotational frequency $\nu = 1/P = 2.789$ day^{-1} ($P = 8.60$ hr). Flanking minima spaced by $\Delta\nu \approx 0.1$ day^{-1} are artifacts of aliasing caused by the data-free gap between the mid-June and late-June observations. Viewed at higher temporal resolution, the PDM plot shows additional alias structure with frequency spacing $\Delta n \approx 1/130$ days, caused by the data-free gap between the June and November observations (Fig. 4). We cannot uniquely determine which of these aliases corresponds to the rotation period of Kowal-Mrkos. However, the most likely single-peaked light-curve period is found at

$$P_L = 8.60 \pm 0.05 \text{ hr} . \quad (5)$$

The phased, composite light curve produced at period P_L is less good than one phased at $2P_L$, leading us to conclude that the light curve of Kowal-Mrkos is double peaked, with period

$$P = 17.21 \pm 0.10 \text{ hr} . \quad (6)$$

The light curve would be expected to have two maxima if produced by rotation of an asymmetric, prolate body about a minor axis. We interpret the double-peaked period light curve as the rotational period of the nucleus. The composite light curve phased to this period is shown in Figure 5. The periodic nature of the variation argues strongly for an origin by rotation of the nucleus rather than, for example, irregular outgassing.

The photometric range is

$$\Delta m_R = 0.45 \pm 0.05 \text{ mag} . \quad (7)$$

A lower limit to the axis ratio b/a can be obtained if we assume the rotation axis of the object is perpendicular to our line of sight ($b/a = 10^{-0.4\Delta m_R}$). We find an axis ratio $b/a \sim \frac{2}{3}$ in the sky plane for 143P/Kowal-Mrkos. Assuming

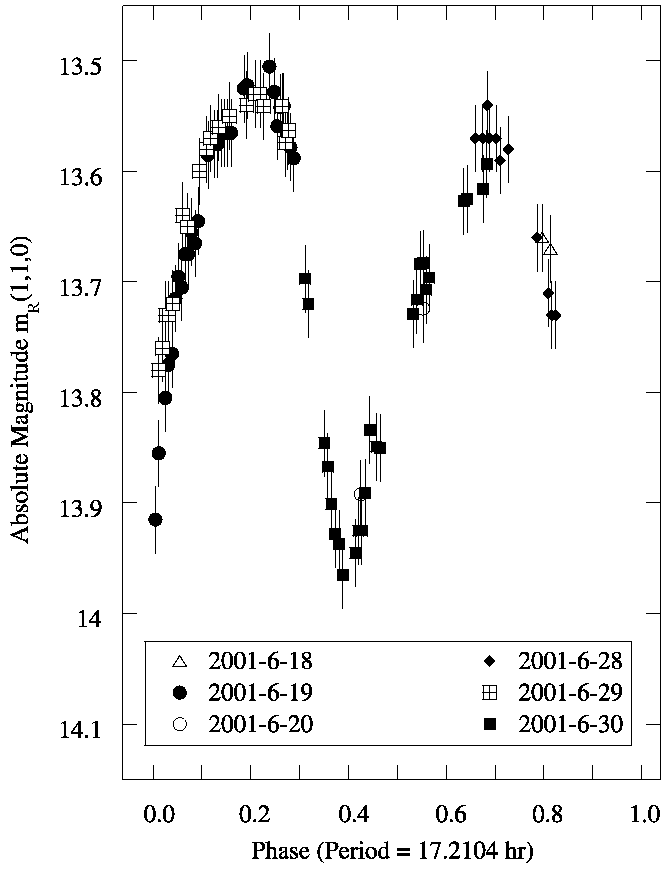

FIG. 5.—Photometry phased to the double-peaked period $P = 17.21035$ hours.

TABLE 3
BROADBAND COLORS OF 143P/KOWAL-MRKOS

UT Date (2001)	m_R	$m_B - m_V$	$m_V - m_R$	$m_R - m_I$
June 19.4454	18.54 ± 0.02[a]	0.84 ± 0.02	0.58 ± 0.02	0.55 ± 0.02
June 19.5735	18.49 ± 0.02[a]	0.80 ± 0.02	0.58 ± 0.02	0.57 ± 0.02

[a] The colors have been computed including a correction for the large rotational light curve of this object.

albedo $p_R = 0.04$, the nucleus projection into the plane of the sky is prolate ellipsoidal with semiaxes 7.0×4.7 km. The elongated shape is entirely typical of other cometary nuclei (Jewitt & Meech 1988) and similar to P/Halley (semiaxes 8×4 km; Keller et al. 1987).

The broadband colors of the nucleus were measured near maximum light (Table 3). The colors are redder than the average colors of cometary nuclei (e.g., $V-R = 0.45 \pm 0.02$ [Jewitt 2002] compared with $V-R = 0.58 \pm 0.02$ for 143P/Kowal-Mrkos) but show no evidence of the ultrared matter detected on the surfaces of many of the supposed JFC parent Kuiper belt objects and Centaurs (Jewitt 2002). This is consistent with a simple model in which the ultrared matter, itself a product of prolonged cosmic-ray processing of organics, is buried on the nuclei of JFCs by a rubble mantle.

4. DISCUSSION OF 143P/KOWAL-MRKOS

A crude empirical limit to the dust mass-loss rate from Kowal-Mrkos can be set using the results derived in § 3 and the formalism described in Jewitt (1991). Equation (26) of the latter reference expresses the mass loss (kg s^{-1}) as

$$\frac{dM}{dt} = \frac{7.5 \times 10^{19} \rho \bar{a} R^{3/2} \Delta 10^{0.4(m_\odot - m_c)}}{\theta p_R \Phi(\alpha)} , \qquad (8)$$

in which ρ is the bulk density of the grains, $\bar{a}$ is their mean radius, θ (arcsec) is the photometry aperture radius, m_c is the effective magnitude of the coma, and the other symbols are already defined. We take $\rho = 10^3$ kg m^{-3}, $\bar{a} = 10^{-6}$ m (see discussion in Jewitt 1991), $R = 3.40$ AU, $\Delta = 2.47$ AU, $\alpha = 8\farcs2$ (Table 1), $\Phi(\alpha) = 10^{-0.4\beta\alpha} \sim 0.5$, and $m_c \geq 21.8$, giving $dM/dt \leq 2$ kg s^{-1}. The fraction of the nucleus surface that must be occupied by water ice to supply dM/dt is

$$f = \frac{dM/dt}{4\pi r_n^2 \, dm/dt} , \qquad (9)$$

where dm/dt (kg m^{-2} s^{-1}) is the specific sublimation rate. We estimate dm/dt by solving the energy-balance equation for a sublimating ice surface,

$$\frac{S_\odot (1-A)}{R^2(t)} = \chi \left[\epsilon \sigma T^4(R) + L(T) \frac{dm(t)}{dt} \right] \qquad (10)$$

(cf. Cowan & A'Hearn 1979).

In equation (10), $S_\odot = 1360$ W m^{-2} is the solar constant, $A = 0.04$ is the assumed Bond albedo, $\epsilon = 0.9$ is the wavelength-averaged emissivity, and $\sigma = 5.67 \times 10^{-8}$ W m^{-2} K^{-4} is the Stefan-Boltzmann constant. The constant χ describes the distribution of incident solar power over the surface of the nucleus. A value of $\chi = 1$ corresponds to a flat plate oriented perpendicular to the Sun; $\chi = 4$ corresponds to an isothermal sphere. We used $\chi = 2$ as an intermediate case, corresponding to a nucleus in which solar energy is both absorbed and emitted entirely from a single hemisphere (i.e., the night side is assumed to be at 0 K). The latent heat of sublimation at temperature $T(R)$ (in kelvins), $L(T)$, is taken from a polynomial approximation to thermodynamic data by Delsemme & Miller (1971):

$$L(T) = 2.875 \times 10^6 - (1.111 \times 10^3 T) . \qquad (11)$$

The temperature dependence of the sublimation rate is obtained from experimental results by Washburn (1926, p. 210).

For $R = 3.4$ AU (Table 1), equation (10) gives $dm/dt = 2.0 \times 10^{-6}$ kg m^{-2} s^{-1}. Substituting in equations (8) and (9), we obtain $f \leq 3 \times 10^{-3}$. While pathological distributions of active areas (e.g., semipermanently shadowed polar regions) could allow a larger f while showing no evidence for mass loss, it seems clear that 143P/Kowal-Mrkos is either a very weakly or an inactive comet. Our observations leave open the possibility that f is a dynamic parameter that adjusts to the insolation on timescales comparable to or even shorter than an orbital period. Future observations near perihelion will place stringent constraints on this possibility.

Low-activity comets have active fractions $10^{-3} \leq f \leq 10^{-2}$ (A'Hearn et al. 1995). The nondetection of coma in Kowal-Mrkos indicates an almost completely mantled surface, at least on the portions of the nucleus that are diurnally exposed to sunlight. We note that the increase in the perihelion distance caused by Jupiter scattering has decreased the perihelion insolation (by a factor of $\sim$6) since the 17th century. Observations of other comets show that outgassing activity is related to changes in their perihelion distance, presumably because of reorganization of the surface mantle in response to a change in the mean insolation (Licandro et al. 2000). The devolatilization of the surface and upper layers while at smaller perihelion distances and the currently lower temperatures (by a factor $6^{-1/4} \sim 0.5$) may be responsible for the absence of outgassing currently displayed by this object. The low (in fact, immeasurable) activity in the present data further builds confidence that the measured *BVRI* colors refer to the nucleus and not to near-nucleus dust. The colors (Table 3) are redder than the median JFC nucleus color, but less red than many Kuiper belt objects and Centaurs (Jewitt 2002). Most probably, the nucleus of Kowal-Mrkos is debris or a ballistic mantle formed by past outgassing of volatiles that were once exposed to solar heat.

5. SHAPES OF COMETARY NUCLEI

The JFCs were long assumed to have been captured from the long-period comet population after formation by gentle

agglomeration in the protosolar disk, followed by a long period of storage in the Oort cloud. Fernández (1980) argued that an origin in a flattened disklike region beyond Neptune was more probable, and the first member of this Kuiper belt was discovered in 1992 (Jewitt & Luu 1993). Now, the nuclei of JFCs are widely considered to be fragments produced collisionally in the Kuiper belt (Farinella & Davis 1996). We first examine whether the shapes of the cometary nuclei are consistent with their origin as fragments produced in energetic collisions between Kuiper belt objects.

Table 4 contains a list of the most reliable observations of cometary nuclei culled from the scientific literature, while Table 5 presents orbital and other data for each. The nucleus shape constraints are primarily derived from measurements of rotational light curves, as in the present case for 143P/Kowal-Mrkos. The distribution of the apparent axis ratios from Table 4 is plotted in Figure 6.

The shapes of fragments produced in laboratory impact experiments have been measured independently by a number of investigators (Catullo et al. 1984; Capaccioni et al. 1984; Giblin et al. 1998). The differences between these measurements are minor and apparently reflect differences in the experimental procedures employed. Here we use the data from Catullo et al. (1984), but we could equally well employ results from the other two papers. Comparison of Figures 6 and 7 shows that the cometary and impact fragment shape distributions are not alike, with a larger mean amplitude for the cometary nuclei.

The small main-belt asteroids (SMBAs) are collisionally produced fragments of precursor bodies. Therefore, the shape distribution of SMBAs provides another reference for comparison with the cometary nuclei. The shape distribution of SMBAs similar in size to the cometary nuclei

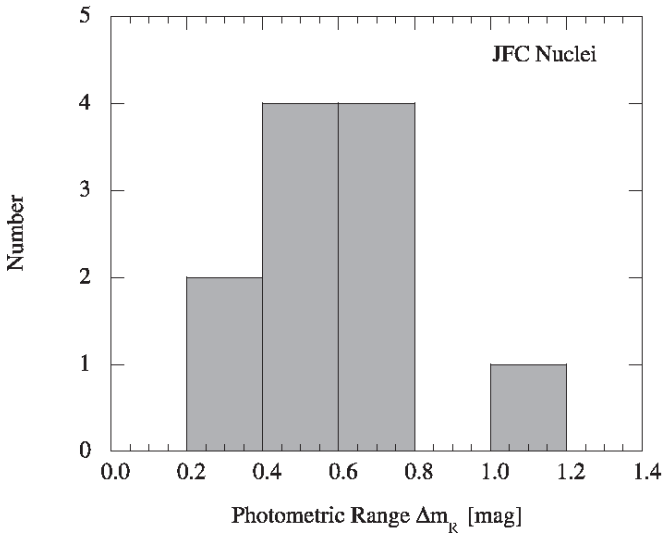

FIG. 6.—Histogram of the photometric range measured in 11 JFC nuclei. Data from Table 4.

(1 km $\leq D \leq$ 6 km) is plotted in Figure 8 (from an unbiased sample by Binzel et al. 1992). Comparison of Figures 7 and 8 shows that the asteroids and laboratory impact fragments, as expected, show similar distributions of axis ratio. However, Figures 6 and 8 show that there is a clear difference between the shape distributions of the collisionally produced SMBAs and the cometary nuclei, with an excess of highly elongated nuclei relative to SMBAs (cf. Jewitt & Meech 1988). These results are summarized in Table 6. What could be the cause of the elongated shapes of the cometary nuclei?

TABLE 4
NUCLEUS PARAMETERS

Comet	$m_R(1, 1, 0)$[a] (mag)	Radius[b] (km)	Δm_R[c] (mag)	b/a[d]	P[e] (hr)	Refs.
JFC nuclei:						
2P/Encke	14.5 ± 0.5	2.4 ± 0.3	0.62 ± 0.05	0.56 ± 0.03	15.08 ± 0.08	1, 2
9P/Tempel 1	14.9 ± 0.3	2.6 ± 0.2	0.6 ± 0.2	0.58 ± 0.10	41.5 ± 0.5	3, 4
10P/Tempel 2	14.3 ± 0.1	5.8 ± 0.5	0.7 ± 0.1	0.52 ± 0.05	8.95 ± 0.01	5
19P/Borrelly	15.0 ± 0.1	2.8 ± 0.3	1.0 ± 0.2	0.40 ± 0.07	25.0 ± 0.5	6
22P/Kopff	15.4 ± 0.1	2.3 ± 0.3	0.45 ± 0.05	0.66 ± 0.05	12.91 ± 0.05	7
28P/Neujmin 1	12.2 ± 0.2	9.7 ± 0.8	0.5 ± 0.1	0.63 ± 0.05	12.67 ± 0.05	8, 9, 10
31P/Schwassmann-Wachmann 2	14.64 ± 0.06	3.1 ± 1.0	0.5 ± 0.1	0.63 ± 0.05	5.58 ± 0.03	11
46P/Wirtanen	18.35 ± 0.10	0.60 ± 0.02	0.2 ± 0.05	0.83 ± 0.04	6.0 ± 0.3	12
49P/Arend-Rigaux	13.9 ± 0.1	5.0 ± 0.5	0.7 ± 0.1	0.52 ± 0.05	13.56 ± 0.16	13, 14
107P/Wilson-Harrington	~16.2	2.0 ± 0.3	0.20 ± 0.05	0.83 ± 0.05	6.10 ± 0.05	15, 16
143P/Kowal-Mrkos	13.49 ± 0.20	5.7 ± 0.6	0.45 ± 0.05	0.66 ± 0.03	17.10 ± 0.01	17
Other nuclei:						
1P/Halley	13.7 ± 0.2	5.8 ± 1.0	1.0 ± 0.1	0.40 ± 0.04	52.80 ± 0.01	18, 19
95P/Chiron	6.24 ± 0.02	74 ± 4	0.088 ± 0.003	0.92 ± 0.01	5.92 ± 0.00	20
C/Levy (1991 L3 = 1991 XI)	13.39 ± 0.05	5.8 ± 0.1	0.3 ± 0.1	0.76 ± 0.07	8.34 ± 0.05	21

[a] Absolute magnitude.
[b] Radius of a spherical body having the same mean cross section as the nucleus.
[c] Light-curve range.
[d] Sky-plane axis ratio, computed from eq. (12).
[e] Nucleus rotation period.

REFERENCES.—(1) Luu & Jewitt 1990; (2) Fernández et al. 2001; (3) Meech 2000; (4) Fernández et al. 2003; (5) Jewitt & Luu 1989; (6) Lamy, Toth, & Weaver 1998b; (7) K. J. Meech 2001, private communication; (8) Jewitt & Meech 1988; (9) Delahodde et al. 2001; (10) Campins et al. 1987; (11) Luu & Jewitt 1992; (12) Lamy et al. 1998a; (13) Jewitt & Meech 1985; (14) Millis et al. 1988; (15) Osip, Campins, & Schleicher 1995; (16) Campins et al. 1995; (17) this work; (18) Jewitt & Danielson 1984; (19) Keller et al. 1987; (20) Bus et al. 1989; (21) Fitzsimmons & Williams 1994.

TABLE 5
NUCLEUS TIMESCALES

Comet	q[a] (AU)	e[b]	a[c] (AU)	Period[d] (yr)	$\overline{dm/dt}$[e] (kg m^{-2} s^{-1})	τ_s[f] (yr)	τ_{ex}[g] (yr)
JFC nuclei:							
2P/Encke	0.339	0.843	2.217	3.3	7.3×10^{-5}	550	48
9P/Tempel 1	1.500	0.519	3.118	5.5	1.1×10^{-5}	3940	140
10P/Tempel 2	1.463	0.528	3.096	5.5	1.2×10^{-5}	7780	2900
19P/Borrelly	1.358	0.624	3.610	6.9	9.7×10^{-6}	4810	300
22P/Kopff	1.584	0.543	3.467	6.5	8.5×10^{-6}	4510	450
28P/Neujmin 1	1.552	0.776	6.919	18.3	2.5×10^{-6}	65,000	2200
31P/Schwassmann-Wachmann 2	3.409	0.195	3.831	7.6	1.1×10^{-6}	47,000	14500
46P/Wirtanen	1.059	0.658	3.095	5.5	1.7×10^{-5}	590	32
49P/Arend-Rigaux	1.369	0.612	3.524	6.7	9.9×10^{-6}	8420	1700
107P/Wilson-Harrington	0.997	0.623	2.643	4.3	2.5×10^{-5}	1330	240
143P/Kowal-Mrkos	2.546	0.409	4.310	9.0	1.9×10^{-6}	50,000	9300
Other nuclei:							
1P/Halley	0.586	0.967	17.833	75.8	1.8×10^{-6}	53,700	3300
95P/Chiron	8.455	0.384	13.741	51.3	~ 0	$\sim\infty$	$\sim\infty$
C/Levy (1991 XI)	0.987	0.929	13.853	51.9	1.8×10^{-6}	53,700	21,000

[a] Perihelion distance.
[b] Eccentricity.
[c] Semimajor axis.
[d] Orbital period.
[e] Average mass loss per unit area per unit time.
[f] Sublimation timescale.
[g] Rotation excitation timescale.

5.1. *Amplitude Bias*

A bias exists in favor of the reporting of highly aspherical nuclei. Their light curves are more interesting than the flat light curves of spherical nuclei and hence more likely to be written up for publication. However, underreporting of flat light curves cannot explain the existence of cometary axis ratios that are larger than any found in the fragment distribution. We conclude that the relative asphericity of the nuclei is unlikely to be caused by this amplitude bias.

In this paper we have conservatively omitted observations of certain nuclei from Table 4, on the grounds that the shape constraints are less directly obtained or simply less convincing than those in our sample. Omitted objects include comets IRAS-Araki-Alcock (1983d) ($b/a = 0.43$; Sekanina 1988), 45P/Honda-Mrkos-Pajdušáková ($b/a \leq 0.77$; Lamy et al. 1999), Machholz 1 ($b/a = 0.7$; K. J. Meech, unpublished), and 29P/Schwassmann-Wachmann 1 ($b/a = 0.38$; Meech et al. 1993). However, it is quite likely that additional data will prove some of these light curves to be accurate. Inclusion of any or all of these objects in Table 4 would enhance, not diminish, the difference with the SMBAs.

5.2. *Limb-darkening Bias*

The ratio of the axes, b/a, is estimated from

$$b/a = 10^{-0.4\Delta m_R}\ , \qquad (12)$$

where Δm_R is the full range of the light curve. This is just the

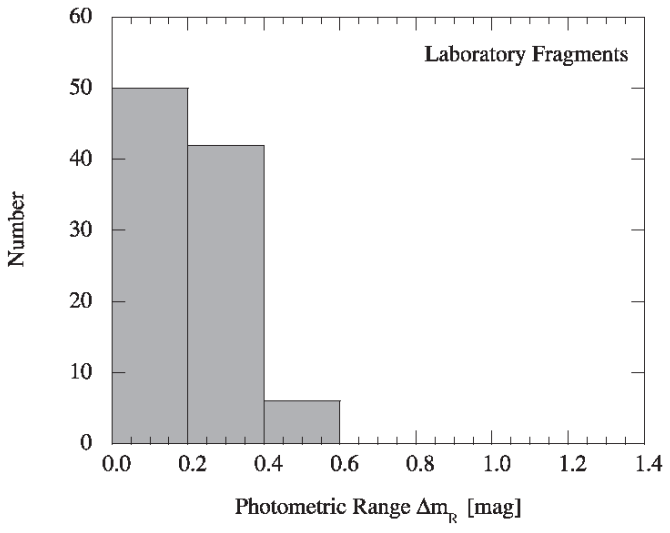

FIG. 7.—Histogram of the photometric range of fragments produced by impact in the laboratory. Data from Catullo et al. 1984.

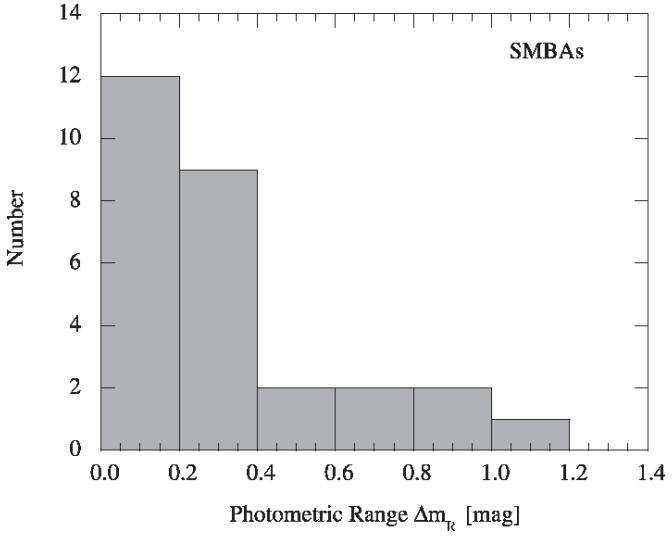

FIG. 8.—Histogram of the photometric range in an unbiased sample of small main-belt asteroids (SMBAs). Data from Binzel et al. 1992.

TABLE 6
AMPLITUDES AND PERIODS COMPARED

Sample	P^a	$\Delta m_R{}^b$	N^c	Source
JFC nuclei.....	15.0 ± 3.1 (12.9)	0.54 ± 0.07 (0.50)	11	This work
SMBA	7.2 ± 0.8 (5.7)	0.32 ± 0.05 (0.20)	28	Binzel et al. 1992
NEO	18.6 ± 8.9 (6.0)	0.52 ± 0.07 (0.41)	25	Pravec, Wolf, & Šarounová 1998

NOTE.—Numbers with error bars are the means and standard deviations on the means. Numbers in parentheses are medians.
[a] Rotation period in hours.
[b] Light-curve range in magnitudes.
[c] Number of objects in the sample

ratio of the geometric cross sections measured at minimum and maximum light and ignores the possible influence of limb darkening. On an elongated body, the magnitude of the limb darkening varies with rotational phase. For plausible convex shapes, a larger fraction of the cross section is near the limb when viewed along the major axis (minimum light) than when viewed perpendicular to that axis (maximum light). Therefore, limb darkening should preferentially diminish the scattered intensity at minimum light, creating a rotational amplitude systematically larger than expected on the basis of equation (12). In other words, blind application of equation (12) will tend to overestimate the axis ratio, b/a, by an amount that depends on the magnitude of the limb darkening and on b/a itself. The possibility of a bias arises in the present study because the limb-darkening coefficients of the nuclei may be systematically different from those of the asteroids and other objects with which they are compared. In particular, the nuclei have smaller albedos than almost all other solar system bodies and will experience a systematically different degree of limb darkening.

We believe that this bias is unimportant for two reasons. First, the magnitude of the effect is small. Laboratory work with meteorite analogs shows that for $\Delta m_R \leq 1$ mag, the differential phase darkening between C-type (low albedo) and S-type (high albedo) asteroids is only $\delta(b/a) \sim 0.05$ (French & Veverka 1983, tending to $\delta(b/a) = 0$ at $\Delta m_R = 0$. For most objects in Table 4, this is comparable to or smaller than the formal uncertainty in the determination of b/a and so can be neglected. Secondly, low-albedo surfaces show less limb darkening than high-albedo surfaces. The bias makes reflective objects appear more elongated than their true axis ratios but has little effect on the low-albedo comets. This is opposite the effect observed, in which the darkest objects (the comets) are the most elongated. Therefore we conclude that the limb darkening bias cannot be the cause of the systematically larger rotational amplitudes seen in the cometary nuclei.

5.3. *Albedo Variations*

The rotational light curves are interpreted as being geometric in origin, but in principle, they could also be influenced by surface albedo variations. Hemispherically averaged albedos varying with rotation by a factor of 2 would mimic a nucleus with axis ratio $b/a = \frac{1}{2}$. Such large albedo variations are rare on the small bodies of the solar system, except for a few pathological objects (e.g., Saturnian satellite Iapetus) that are of questionable relevance to the case of the cometary nuclei. Several considerations suggest that hemispheric albedo variations are not an important source of error. In the cases of 1P/Halley (Keller et al. 1987) and 19P/Borrelly (Soderblom et al. 2002), we possess in situ, high-resolution images that confirm the geometric interpretation of the light curve. For comets 10P/Tempel 2, 28P/Neujmin 1, and 49P/Arend-Rigaux, we possess time-resolved measurements of the albedo that show no significant variation with rotational phase (A'Hearn et al. 1989; Campins, A'Hearn, & McFadden 1987; Millis, A'Hearn, & Campins 1988). For the other nuclei in Table 4, we possess no direct evidence against albedo modulation of the brightness. However, the light curves show two-peaked asymmetries that are naturally explained as geometric effects caused by pear-shaped bodies. For these reasons, while we cannot rule out the effects of albedo variations on all nuclei, we are confident that albedo does not play a dominant role in shaping the light curves.

5.4. *Sublimation Modification*

Sublimation naturally exaggerates the asphericity of nonspherical nuclei even if the sublimation proceeds uniformly over the surface. To see this, consider a prolate spheroidal nucleus with initial semiaxes $a_0 > b_0 = c_0$. We suppose that the longest dimension of the nucleus shrinks to zero in characteristic time τ_s, so that the distance moved by the sublimation front in time t is $a_0 t/\tau_s$. Then, in uniform sublimation, we may write

$$\phi(t/\tau_s) = \frac{\phi(0) - t/\tau_s}{1 - t/\tau_s} \tag{13}$$

for the time dependence of the axis ratio, where $\phi(0) = b_0/a_0$. Equation (13) is valid provided that $\phi(t/\tau_s) \geq 0$.

Solutions to equation (13) are shown with solid lines in Figure 9 for $\phi(0) = 0.6$, 0.8, and 1.0. We also plot in Figure 9 the fraction of the initial mass that has been ejected from the nucleus as a function of time (*dashed lines*). The figure shows that, for the pathological case $\phi(0) = 1$ (a sphere), the nucleus shape is constant, as expected. For other shapes, $\phi(t/\tau_s)$ decreases sharply with time. For example, take a collisionally produced nucleus with shape corresponding to the median of the measured axis ratios of the SMBAs, namely, $\phi(0) \sim 0.8$ (Table 6). Then, to evolve through uniform sublimation to $\phi(t/\tau_s) = 0.63$, corresponding to the median axis ratio of the JFC nuclei (Table 6), we require $t/\tau_s \sim 0.4$. During this time, the long axis has shortened by 40% and about 90% of the mass of the nucleus has been ejected. Equation (13) and Figure 9 clearly show that elongated nucleus shapes are a consequence of uniform sublimation.

Prolonged anisotropic mass loss might deform the nuclei even faster. Evidence that cometary mass loss is largely anisotropic is provided by numerous observations of jets and

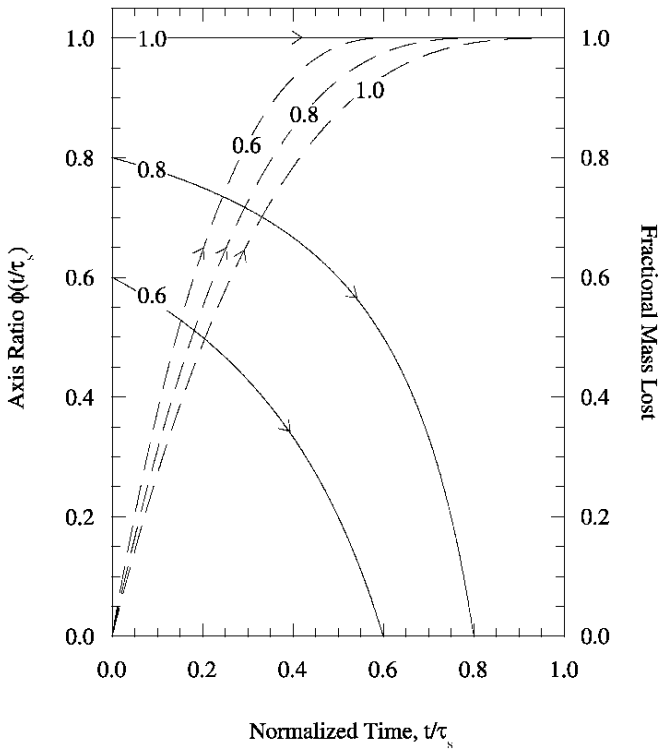

FIG. 9.—Time evolution of the nucleus axis ratio (*solid lines*) and the fraction of the nucleus mass that is lost (*dashed lines*) for a model of a uniformly sublimating prolate spheroidal nucleus. Numbers on the curves identify the initial axis ratios $\phi(0) = 0.6$, 0.8, and 1.0. Time is expressed in units of the sublimation lifetime, τ_s (see eq. [14]).

other structures in the inner comae, and by the existence of nongravitational accelerations whose origin lies in anisotropy (Whipple 1950). Strictly, we do not know the lifetimes of the vents that produce outgassing anisotropy, so it is possible that vent migration averages out the anisotropy over long periods. In any case, sustained anisotropic mass loss can only add to the tendency of the nucleus to grow more elongated with time.

The rate of shrinkage of a spherical nucleus of radius r_n is related to the specific sublimation rate by $dr_n/dt \sim -(dm/dt)/\rho$, where ρ (kg m^{-3}) is the bulk density. The timescale for free sublimation to excavate a concavity of depth equal to half the nucleus radius is just $\tau_s \sim r_n/(2dr_n/dt)$, or

$$\tau_s \sim \tfrac{1}{2}\rho r_n(\overline{dm/dt})^{-1} , \qquad (14)$$

where $\overline{dm/dt}$ is the mass loss rate per unit area averaged around the orbit.

We calculated τ_s for each of the nuclei in Table 4 and list the results in Table 5. The mass-loss rate, dm/dt, was integrated around the orbit by solving Kepler's equation and applying equations (10) and (11) at each point. For this purpose we again used $A = 0.04$ and $\chi = 2$. The results provide a measure of the sublimation lifetime for the comets in their present orbits. The JFC orbits evolve chaotically on timescales of ~1000 yr (Tancredi 1995), short compared with τ_s. Mantle growth on the comets can restrict the loss of volatiles, lengthening the time needed to modify the shape. Vents of substantial depth might become self-shadowing, cutting off the sublimation. Nevertheless, we see that for the JFC nuclei (Table 5) the resulting sublimation times, 500 yr $\leq \tau_s \leq$ 65,000 yr, are all less than the median dynamical

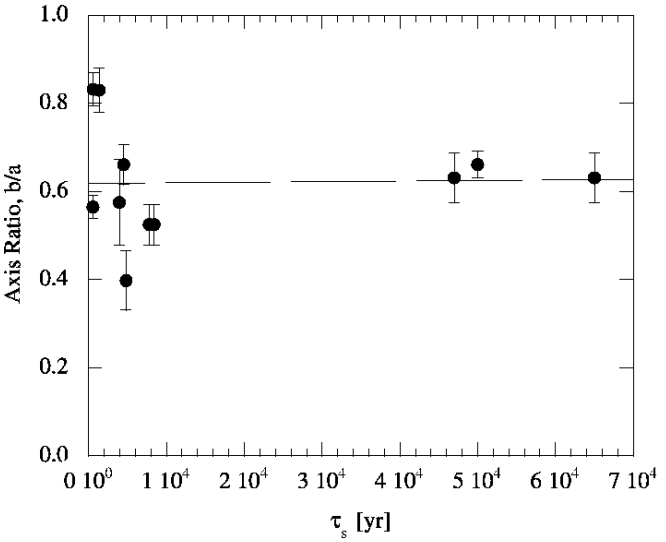

FIG. 10.—Axis ratio b/a plotted against sublimation timescale τ_s. The line shows a least-squares fit to the data. Data from Tables 4 and 5.

lifetime $\tau_{dyn} \sim 4 \times 10^5$ yr of the population (Levison & Duncan 1994). This shows that mass loss cannot be ignored as a possible agent for reshaping the nuclei.

The search for evolution of the shapes of the cometary nuclei is seriously hampered by the inability to assign a dynamical age (i.e., a time since entry into the planetary region) to any nucleus. As remarked above, the orbital evolution is chaotic. However, in a probabilistic sense, the nuclei with short τ_s are more likely to have suffered shape modification by sublimation than are those with long τ_s. Therefore, as a simple test for the effects of mass loss on nucleus shape, we examine the axis ratio as a function of τ_s. Figure 10 shows no evidence for any dependence of b/a on τ_s. The linear correlation coefficient is $R_{cor} = 0.026$ ($N = 11$), and the probability that this or a larger R_{cor} might be obtained by chance from uncorrelated data is $P(0.026, 11) \geq 0.1$.

5.5. *Rotational Deformation*

Asymmetric mass loss from a cometary nucleus imposes a torque that can change the spin vector. Spin-up of a low tensile strength nucleus could result, in principle, in rotational deformation along the Jacobi-Maclaurin spheroid series and even disruption if the centripetal limit is exceeded. The timescale for spin excitation is

$$\tau_{ex} \sim \frac{\omega\rho r_n^4}{V_{th}k_T\, dM/dt} , \qquad (15)$$

where dM/dt is the net mass loss rate from all vents, $\omega = 2\pi/P$ is the angular frequency, and V_{th} is the mass-weighted outflow speed (cf. Samarasinha et al. 1986; Jewitt 1991). The quantity k_T is the dimensionless moment arm for the torque, which is a function of the angular pattern of the emission from the nucleus. The value $k_T \sim 0.05$ has been estimated from simple models and is probably uncertain by at least a factor of several (Jewitt 1997).

We have estimated values of the spin excitation time for each of the nuclei in Table 4 using equation (15) applied to the specific sizes, rotational periods, and orbits. We used equation (9) to estimate the total mass-loss rate with

assumed mantle fraction $f = 0.01$ (cf. A'Hearn et al. 1995). The specific mass loss rate dm/dt was evaluated around the orbit of each comet using equations (10) and (11). The resulting values of τ_{ex} are listed in Table 5 for each nucleus. The table shows that the spin excitation times are all very short compared with the dynamical lifetimes, within the uncertainties of our simplistic model. Again, the listed timescales provide only a qualitative guide. If the vent lifetimes are short compared with τ_{ex}, then the applied torque would stop and start as vents appear and die, perhaps giving a (much slower) random walk toward breakup. Nevertheless, the excitation timescales in Table 5 are very short, showing that we must be alert to the possibility of a spin-shape relation.

Once again, while we cannot assign definite dynamical ages to particular comets, it is reasonable to expect that nuclei with small τ_{ex} are the most likely to have been spun up. The relation between b/a and τ_{ex} is shown in Figure 11. The linear correlation coefficient is $R_{cor} = 0.014$ ($N = 11$), and the probability that this or a larger value might arise by chance from uncorrelated data is $P(0.014, 11) \geq 0.1$. We also searched for correlations between b/a and the rotation period [$R_{cor} = 0.489$ ($N = 11$), $P(0.489, 11) \geq 0.1$] and between b/a and the rotational stress, which scales as $(r_n/P)^2$ [$R_{cor} = 0.077$ ($N = 11$), $P(0.077, 11) \geq 0.1$]. In no case is there evidence for a statistically significant correlation.

The median rotation period of the cometary nuclei ($P = 12.9$ hr) is twice the values for either the SMBAs ($P = 5.7$ hr) or the near-Earth objects (NEOs: $P = 6.0$ hr; see Table 6). The critical period for rotational breakup of small, strengthless asteroids is near $P_c \sim 2.2$ hr (Pravec & Harris 2000), and this period varies as $P_c \propto \rho^{-1/2}$. The lower mean densities of the cometary nuclei (e.g., $\rho \sim 300$–600 kg m^{-3}, compared with $\rho \sim 2000$ kg m^{-3} for the asteroids) imply critical periods for rotational breakup longer by a factor of $\sim$1.8–2.6, corresponding to $P_c \sim 4.0$–5.7 hr for the comets. This might explain the absence of shorter periods among the known comets and bias the mean toward higher values. The longer periods of the surviving comets may mean that rotational elongation is unimportant for these objects.

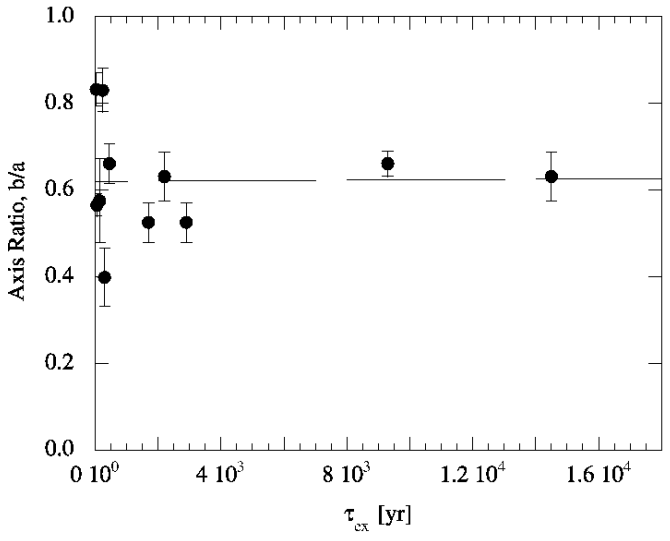

FIG. 11.—Axis ratio b/a plotted against the spin excitation timescale τ_{ex}. The line shows a least-squares fit to the data. Data from Tables 4 and 5.

6. DISCUSSION

We consider possible explanations of the results from the previous section.

1. The NEOs have mean axis ratios b/a more similar to those of the comets than to the main-belt asteroids from which they are derived (Table 6). Apart from the obvious explanation that some of the NEOs are themselves dead comets, it has been suggested that the NEOs have been stretched by tidal interactions with the terrestrial planets (Richardson, Bottke, & Love 1998). The efficiency of spin-up and elongation by tidal torques is enhanced by rapid rotation. The longer median rotation period of the comets (Table 6) reduces the likelihood that tidal torques might explain their extreme shapes. Moreover, the timescale for encounters that are close enough to modify the shapes of (assumed strengthless) NEOs is $\sim$65 Myr (Richardson et al. 1998), which is comparable to the $\tau_{dyn} \sim 20$ Myr dynamical lifetime of the NEOs (Gladman et al. 1997) but $\sim 10^2$ times τ_{dyn} for the JFCs. Tidal stretching during interactions with the terrestrial planets is likely to be important for, at most, $\sim$1% of the comets. During their previous lives as Centaurs, the JFCs had a comparably small probability of passing within the Roche radii of the giant planets. We conclude that elongation through tidal interactions with planets is likely to be insignificant.

2. If taken at face value, the absence of a correlation between b/a and either τ_s or τ_{ex} could mean that nucleus shapes are unaffected by sublimation and spin-up. This would be difficult to understand, however, in view of the profound loss of mass known to occur from the comets (Hughes & McBride 1989; Jenniskens & Betlem 2000). Table 7 summarizes the parameters of five meteoroid streams and their parents and indicates that the mean fraction of the total mass contained in the streams is $M_s/(M_s + M_p) = 0.21 \pm 0.06$. In other streams where the parent is not known, this fraction may approach unity. The point is that comets lose a substantial fraction of their initial mass. This is the key process needed to produce an elongated nucleus from an initially more round one (cf. Fig. 9).

3. For these reasons, we prefer the alternate explanation of Figures 10 and 11, namely, that there is no measurable correlation because the timescale for losing mass and changing the shape is so short that all of the nuclei in our sample have already been modified. This is suggested by Table 5, which shows that $\tau_s \leq 0.1\tau_{dyn}$ for the JFC comets. We should expect $\leq 1/10$ of a random sampling of comets to be so dynamically young as to be relatively free from the effects of mass loss. In a sample consisting of only 11 nuclei, perhaps one might preserve any record of its initial shape. Our sample is far from random, however. The observed comets are mostly low-activity objects selected on the basis of the observability of their nuclei against the confusing background coma. Therefore, it is likely that the nuclei studied here are more evolved than average, and that the elongated shapes represent some sort of end state in the shape modification process. Progressive mantling of the comets, for which the timescale is likely to be short, provides a natural explanation of the cessation of mass loss and the "freezing in" of elongated shapes in the present sample.

TABLE 7
COMET AND DEBRIS MASSES

Quantity	Quadrantid	Perseid	Orionid	Geminid	Leonid
Parent object	5496	109P	1P	3200	55P
Parent type[a]	Asteroid	Comet	Comet	Asteroid	Comet
Parent radius[b]	1.8	10.5	5.0	2.6	1.8
Parent mass M_p[c]	1.2×10^{13}	2.4×10^{15}	2.6×10^{14}	3.7×10^{13}	1.2×10^{13}
Stream mass M_s[d]	1.3×10^{12}	3.1×10^{14}	3.3×10^{13}	1.6×10^{13}	5.0×10^{12}
$M_s/(M_s + M_p)$[e]	0.10	0.13	0.13	0.38	0.29

NOTE.—Stream parameters are from Hughes & McBride 1989 and Jenniskens & Betlem 2000.
[a] The asteroid classification only means that the parent does not now show a coma. Presumably, objects classified as asteroids are dead or dormant comets.
[b] Estimated nucleus radius in kilometers.
[c] Estimated nucleus mass in kilograms, computed assuming a spherical shape and density $\rho = 500$ kg m^{-3}.
[d] Meteor stream mass in kilograms.
[e] Fraction of the total mass contained within the meteor stream.

6.1. *Predictions and Future Work*

If the shapes of the comets reflect their collisional origin in the Kuiper belt followed by sublimation-driven mass loss once inside the orbit of Jupiter, then we can make two direct, observationally testable predictions.

First, we predict that the small KBOs and Centaurs should have average shapes consistent with those of collisionally produced fragments, namely, $\overline{\Delta m_R} = 0.32 \pm 0.05$ (Table 6). This prediction should be tested using the more distant, nonsublimating members of the KBO and Centaur populations with sizes (1 km $\leq D \leq$ 10 km) comparable to the well-studied cometary nuclei. To date, constraints on the shapes of only the largest KBOs (diameters $D \geq 100$ km) are available (Sheppard & Jewitt 2002). These objects are not collisionally produced fragments and thus cannot be meaningfully compared with the present nucleus sample.

Second, we predict that the dead comets should have average shapes like those of the nuclei, namely, $\overline{\Delta m_R} = 0.54 \pm 0.07$. Recent work has shown that asteroids with comet-like dynamical characteristics (principally, Tisserand parameters $T_J < 3$) also possess comet-like albedos (Fernández et al. 2001). Thus, we predict that the light curves of the dynamical counterparts of the JFCs, namely, the $2 < T_J < 3$ asteroids, will be indistinguishable from those of the JFC comets.

Independently of these two predictions, there is a clear need for larger samples of well-characterized cometary nuclei in the Jupiter family, Halley family, and long-period dynamical groups. Based on past experience, the effort expended in obtaining these samples will be considerable.

7. SUMMARY

The main results on 143P/Kowal-Mrkos are the following:

1. Deep images show a pointlike morphology in which steady state coma contributes no more than 5% to the total light measured inside a 1″ radius aperture. The nucleus is dead or almost completely inactive, presumably because of mantling by refractory material deposited on the surface by sublimating ices.

2. The mean brightness of the comet varies with phase angle in the range $5^\circ \leq \alpha \leq 12^\circ$, with a phase coefficient $\beta = 0.043 \pm 0.014$ mag deg^{-1}. This is consistent with scattering from a low-albedo surface.

3. The total light from the comet is modulated with a double-peaked period 17.21 ± 0.10 hr, which we interpret to be the rotation period of the nucleus. The photometric range is 0.45 mag, indicating a projected (sky plane) nucleus axis ratio $b/a \sim \frac{2}{3}$.

4. The rotationally averaged absolute magnitude of the nucleus is $m_R(1, 1, 0) = 13.49 \pm 0.20$, corresponding to effective circular radius $r_n = 5.7 \pm 0.6$ km assuming red geometric albedo $p_R = 0.04$. The actual radii of the prolate nucleus projected into the sky plane are 7.0×4.7 km.

5. The colors of 143P/Kowal-Mrkos ($B-V = 0.82 \pm 0.02$, $V-R = 0.58 \pm 0.02$, and $R-I = 0.56 \pm 0.02$) are redder than most Jupiter-family comets, but there is no evidence for the ultrared material seen in Kuiper belt objects and Centaurs.

The main results concerning the shapes of cometary nuclei are the following:

1. The mean of the photometric ranges of 11 well-observed Jupiter-family comet nuclei is $\overline{\Delta m_R} = 0.54 \pm 0.07$. This corresponds to a mean axis ratio, projected into the plane of the sky, $\overline{b/a} = 0.61 \pm 0.04$, for nuclei with approximate diameters 1 km $\leq D \leq$ 20 km.

2. The JFC nuclei are more elongated, as a group, than main-belt asteroids of comparable size, as found earlier by Jewitt & Meech (1988). The JFC nuclei are also more elongated than fragments produced by catastrophic disruption of targets in the laboratory by impact.

3. Shape modification is a likely outcome of extensive mass loss from the nuclei. Evidence for substantial mass loss is shown by the meteor streams (Table 7). Evidence that mass loss is anisotropic includes the nongravitational accelerations of comets and observations of jet structure in the inner coma.

4. We find no correlation between the nucleus axis ratio and the corresponding timescales for mass loss by sublimation or spin-up by outgassing torques. While this could be explained if the shapes were not determined by mass loss or spin-up, the more likely explanation is that the JFC nuclei in the present sample are the surviving remnants of a highly evolved population.

We thank University of Hawaii telescope operators John Dvorak and Paul deGrood for their help, and NASA's Planetary Astronomy Program for support of this work through a grant to D. J.

REFERENCES

A'Hearn, M. F., Campins, H., Schleicher, D. G., & Millis, R. L. 1989, ApJ, 347, 1155
A'Hearn, M. F., Millis, R. L., Schleicher, D. G., Osip, D. J., & Birch, P. V. 1995, Icarus, 118, 223
Belskaya, I. N., & Shevchenko, V. G. 2000, Icarus, 147, 94
Binzel, R. P., Xu, S., Bus, S. J., & Bowell, E. 1992, Icarus, 99, 225
Bowell, E., Hapke, B., Domingue, D., Lumme, K., Peltoniemi, J., & Harris, A. W. 1989, in Asteroids II, ed. R. P. Binzel, T. Gehrels, & M. S. Matthews (Tucson: Univ. Arizona Press), 524
Bus, S. J., Bowell, E., Harris, A. W., & Hewitt, A. V. 1989, Icarus, 77, 223
Campins, H., A'Hearn, M. F., & McFadden, L.-A. 1987, ApJ, 316, 847
Campins, H., Osip, D. J., Rieke, G. H., & Rieke, M. J. 1995, Planet. Space Sci., 43, 733
Capaccioni, F., et al. 1984, Nature, 308, 832
Carusi, A., Kresák, L., Perozzi, E., & Valsecchi, G. B. 1985, Long-Term Evolution of Short-Period Comets (Bristol: Hilger)
Catullo, V., Zappalá, V., Farinella, P., & Paolicchi, P. 1984, A&A, 138, 464
Cowan, J. J., & A'Hearn, M. F. 1979, Moon Planets, 21, 155
Delahodde, C. E., Meech, K. J., Hainaut, O. R., & Dotto, E. 2001, A&A, 376, 672
Delsemme, A. H., & Miller, D. C. 1971, Planet. Space Sci., 19, 1229
Farinella, P., & Davis, D. R. 1996, Science, 273, 938
Fernández, J. A. 1980, MNRAS, 192, 481
Fernández, Y. R., Jewitt, D. C., & Sheppard, S. S. 2001, ApJ, 553, L197
Fernández, Y. R., et al. 2000, Icarus, 147, 145
Fernández, Y. R., Meech, K. J., Lisse, C. M., A'Hearn, M. F., Pittichova, J., & Belton, M. J. S. 2003, Icarus, in press
Fitzsimmons, A., & Williams, I. P. 1994, A&A, 289, 304
French, L. M., & Veverka, J. 1983, Icarus, 54, 38
Giblin, I., Martelli, G., Farinella, P., Paolicchi, P., Di Martino, M., & Smith, P. N. 1998, Icarus, 134, 77
Gladman, B. J., et al. 1997, Science, 277, 197
Hughes, D. W., & McBride, N. 1989, MNRAS, 240, 73
Jenniskens, P., & Betlem, H. 2000, ApJ, 531, 1161
Jewitt, D. 1991, in IAU Colloq. 116, Comets in the Post-Halley Era, Vol. 1, ed. R. L. Newburn, Jr., M. Neugebauer, & J. Rahe (Dordrecht: Kluwer), 19
———. 1997, Earth Moon Planets, 79, 35
Jewitt, D., & Luu, J. 1989, AJ, 97, 1766
———. 1993, Nature, 362, 730
Jewitt, D., & Meech, K. J. 1985, Icarus, 64, 329
Jewitt, D. C. 2002, AJ, 123, 1039
Jewitt, D. C., & Danielson, G. E. 1984, Icarus, 60, 435
Jewitt, D. C., & Meech, K. J. 1988, ApJ, 328, 974
Keller, H. U., et al. 1987, A&A, 187, 807
Kowal, C. T., & Mrkos, A. 1984, IAU Circ. 3988
Lamy, P. L., Toth, I., A'Hearn, M. F., & Weaver, H. A. 1999, Icarus, 140, 424
Lamy, P. L., Toth, I., Jorda, L., Weaver, H. A., & A'Hearn, M. 1998a, A&A, 335, L25
Lamy, P. L., Toth, I., & Weaver, H. A. 1998b, A&A, 337, 945
Landolt, A. U. 1992, AJ, 104, 340
Laufer, D., Notesco, G., Bar-Nun, A., & Owen, T. 1999, Icarus, 140, 446
Levison, H. F., & Duncan, M. J. 1994, Icarus, 108, 18
Licandro, J., Tancredi, G., Lindgren, M., Rickman, H., & Gil-Hutton, R. 2000, Icarus, 147, 161
Luu, J., & Jewitt, D. 1990, Icarus, 86, 69
Luu, J. X., & Jewitt, D. C. 1992, AJ, 104, 2243
Marsden, B. G. 2000, IAU Circ. 7403
Meech, K. 2000, in ASP Conf. Ser. 213, Bioastronomy '99, ed. G. A. Lemarchand & K. J. Meech (San Francisco: ASP), 207
Meech, K. J., Belton, M. J. S., Mueller, B. E. A., Dicksion, M. W., & Li, H. R. 1993, AJ, 106, 1222
Millis, R. L., A'Hearn, M. F., & Campins, H. 1988, ApJ, 324, 1194
Osip, D., Campins, H., & Schleicher, D. G. 1995, Icarus, 114, 423
Pravec, P., & Harris, A. W. 2000, Icarus, 148, 12
Pravec, P., Wolf, M., & Šarounová, L. 1998, Icarus, 136, 124
Richardson, D. C., Bottke, W. F., & Love, S. G. 1998, Icarus, 134, 47
Samarasinha, N. H., A'Hearn, M. F., Hoban, S., & Klinglesmith, D. A., III. 1986, in Proc. 20th ESLAB Symposium on the Exploration of Halley's Comet, Vol. 1, ed. B. Battrick, E. J. Rolfe, & R. Reinhard (ESA SP-250) (Paris: ESA), 487
Sekanina, Z. 1988, AJ, 95, 1876
Sheppard, S. S., & Jewitt, D. C. 2002, AJ, 124, 1757
Soderblom, L. A., et al. 2002, Science, 296, 1087
Stellingwerf, R. F. 1978, ApJ, 224, 953
Tancredi, G. 1995, A&A, 299, 288
Washburn, E. W., ed. 1926, International Critical Tables of Numerical Data, Physics, Chemistry and Technology, Vol. 3 (New York: McGraw-Hill)
Whipple, F. L. 1950, ApJ, 111, 375